B-DNA Under Stress: Over- and Untwisting of DNA during Molecular Dynamics Simulations

Srinivasaraghavan Kannan, Kai Kohlhoff, and Martin Zacharias
School of Engineering and Science, International University Bremen, Bremen, Germany

ABSTRACT   The twist flexibility of DNA is central to its many biological functions. Explicit solvent molecular dynamics simulations in combination with an umbrella sampling restraining potential have been employed to study induced twist deformations in DNA. Simulations allowed us to extract free energy profiles for twist deformations and were performed on six DNA dodecamer duplexes to cover all 10 possible DNA basepair steps. The shape of the free energy curves was similar for all duplexes. The calculated twist deformability was in good agreement with experiment and showed only modest variation for the complete duplexes. However, the response of the various basepair steps on twist stress was highly nonuniform. In particular, pyrimidine/purine steps were much more flexible than purine/purine steps followed by purine/pyrimidine steps. It was also possible to extract correlations of twist changes and other helical as well as global parameters of the DNA molecules. Twist deformations were found to significantly alter the local as well as global shape of the DNA modulating the accessibility for proteins and other ligands. Severe untwisting of DNA below an average of 25° per basepair step resulted in the onset of a global structural transition with a significantly smaller twist at one end of the DNA compared to the other.

INTRODUCTION

The conformational flexibility of DNA is central to its many biological functions including recognition by proteins during gene regulation, DNA repair, packaging in the cell, and transient melting during transcription and replication (1–6). Specific binding by proteins is not only determined by specific interactions between DNA and proteins but also by the sequence-dependent structure and deformability of the DNA helix (1–4,7–16). In vivo DNA is mostly found in circularly closed form including supercoiling that causes a mechanical stress (torque) on the DNA twist and can strongly affect recognition by proteins and influence transcription and replication fidelity (6,15). Therefore, better understanding of the sequence-dependence of the DNA twist flexibility is of particular interest. The total twist and to some degree also the twist elasticity of DNA can be measured using DNA ring-closure ligation (cyclization) experiments with DNA molecules of different length and including a helix phasing analysis (17–19). This technique has been used to study the twist flexibility of DNA fragments of various length and sequence in solution. Alternatively, time-resolved fluorescence polarization anisotropy (on DNA with intercalated ethidium-bromide) can also be used to measure torsional DNA flexibility near the equilibrium state (20,21). These studies indicate that the overall base composition has only a modest influence on the average twist flexibility of DNA. Recently, it has also become possible to study the elastic response of single DNA molecules upon application of external torques to un- or

over-twisted DNA (22). Such experiments provide valuable insights into the physical and elastic properties of DNA molecules. However, only relatively long DNA molecules (>1 kbp) can be studied that can react on the external stress by local as well as global conformational changes (e.g., supercoiling that relaxes part of the twist-stress). Similar to the DNA ring closure experiments, an overall twist elasticity can be obtained—but with only modest insight provided into the conformational changes taking place at the molecular level.

High-resolution experimental structures of isolated DNA molecules and complexes with organic ligands and proteins allow us to study the fine structure of DNA. Under the assumption that observed structural variations reflect the intrinsic deformability of B-DNA the analysis provides insights into the flexibility of DNA near the native state at atomic resolution including also DNA twist elasticity (3,4,7–15). Olson and co-workers (4) have extensively analyzed structural variations in available DNA oligonucleotide structures and complexes with proteins and were able to derive a sequence-dependent empirical energy function for the DNA helical elasticity. The approach also allows to investigate possible correlations between helical parameters that describe the flexibility of nucleic acids. However, it is not clear how well a set of crystal structures reflects the structural flexibility of DNA in solution.

Alternatively, the progress in molecular mechanics force fields and simulation methodology has made it possible to investigate DNA helical flexibility using molecular dynamics (MD) simulations including surrounding water molecules and ions (reviewed in (23–26)). Such MD simulations of DNA result in stable structures close to the experimental DNA conformations on the nanosecond timescale and can be used to characterize the equilibrium fluctuations of helical

parameters (27–31). Computational large-scale studies on many different DNA molecules have been used to study the sequence-dependence of DNA flexibility and are also helpful to improve the molecular mechanics force fields (32,33). However, unrestrained MD simulations may allow only a limited sampling of possible substates due to energy barriers. To better understand the molecular mechanism of elastic twist deformations in DNA, in the current study, MD simulations combined with a twistlike restraining potential and the umbrella sampling method were used. Simulations were performed on several 12-bp DNA oligo-nucleotides with different sequences and for a range of total twist angles of the central 9-bp steps. The simulations allowed us to calculate the total free energy change, to characterize the twist change of individual basepair steps and to analyze the change of other DNA helical parameters in response to external twist deformations. In addition, the onset of an untwisting transition starting from one end of a DNA helix was observed.

MATERIALS AND METHODS

Simulations were performed on six 12-bp B-DNA molecules (Table 1) with the general sequence (5'-CGCGNNNNCGCG)$_2$ and six different central sequences (AATT, TATA, CGCG, GATC, CATG, CTAG). The central sequences cover each of the 10 possible basepair steps in DNA (AA, GG, GC, AG, TA, CG, CA, GC, AT, GT) at least once. Standard B-DNA start structures were generated using the *Nucgen* program of the AMBER8 package (34). Each system was neutralized by adding 22 K$^+$ counter ions and solvated with ~4500 TIP3P water molecules (35) in a rectangular box using the *xleap* module of AMBER8. The simulation systems were subjected to energy minimization (1000 steps) using the *Sander* module. The PARM99 force field (36,37) was used for all simulations. During MD each DNA was initially harmonically restrained (25 kcal mol^{-1} Å^{-2}) to the energy-minimized start coordinates and the system was heated up to 300 K in steps of 100 K followed by gradual removal of the positional restraints and 1-ns unrestraint equilibration of each system at 300 K. During MD the long-range electrostatic interactions were treated with the particle-mesh Ewald method (38) using a real-space cutoff distance of $r_{\text{cuttoff}} = 9$ Å. The RATTLE algorithm (39) was used to constrain bond vibrations involving hydrogen atoms, which allowed a time step of 2 fs. To introduce the external twist stress, a modified version of the *tornrg* subroutine (which calculates the torsion-angle restraint energy in *Sander*) was used to harmonically restrain a twist angle between the second and eleventh basepair of each 12-bp duplex DNA. This twist angle (in the following termed τ) is formed by the distance vector between C$_1'$ atoms of the 11th basepair projected onto the plane

defined by the distance vector of C$_1'$ atoms of the second basepair and the axis connecting the midpoints of the two pairs of C$_1'$ atoms (see Fig. 1). It is important to note that the above-defined twist-angle is only an approximation to the "real" twist because it is calculated with respect to a linear helical axis along the DNA. To compare the approximate twist restraining coordinate with a more accurate definition that also accounts for a possible curved helical axis, it was compared to the twist obtained using the program *Curves* (40,41). For the range of twist angles considered in this study, a good correspondence was observed (Fig. 2). During restraint MD simulations a quadratic penalty function for deviations of the 9-bp twist with respect to a reference twist value was used. To obtain start structures for the umbrella sampling simulations the reference τ-angles was changed in steps of 5° with an equilibration run of 0.2 ns for each τ. A total τ-range of ~225–360° per 9-bp steps was covered representing a range of ~25–40° per basepair step. The twist along the central 9-bp steps after the unstrained equilibrium simulations was ~292° (corresponding to ~32.5° per bp step and depending slightly on the sequence). The total τ-range of ~225–360° per 9-bp steps represents a twist deformation of ~±70° per 9 bp steps (or ±7.5° per bp step) with respect to the equilibrium twist. During the equilibration the central basepair was weakly positionally restrained (force constant 0.01 kcal mol^{-1} Å^{-2}). This does not affect the internal dynamics of the basepair to any significant extent but avoids any overall rotation of the DNA and keeps the helical axis approximately aligned with the long axis of the rectangular box. Subsequently, however, during 1-ns data gathering for each reference τ-angle, the DNA was completely free to move except for the twist restraint. The actual restraining twist angle was recorded every 10 simulation steps. Complete coordinate frames were stored every 2 ps. The potential of mean force (PMF) along the reaction coordinate was calculated using the weighted histogram analysis (WHAM) method (42,43). Helical and dihedral angle parameters of recorded structures were calculated using *Curves* (40,41).
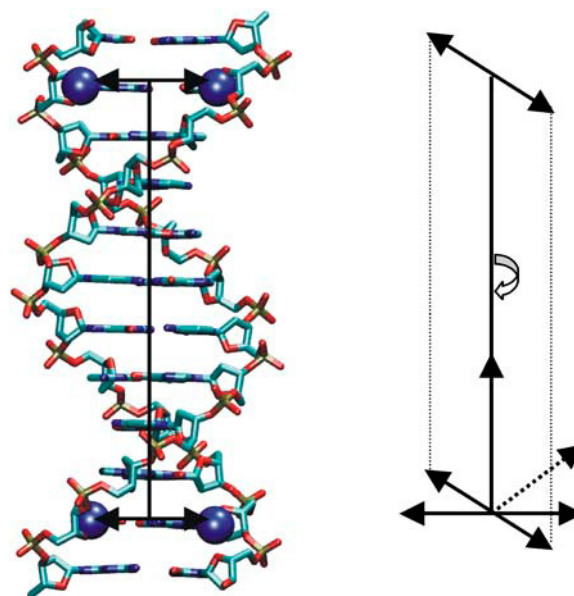

FIGURE 1 Definition of the twist-restraining coordinate. The twist-restraining angle (termed τ) is formed by the distance vector (*upper double arrow*) between C1' atoms (*blue spheres* in the *left panel*) of the 11th basepair projected onto the plane defined by the distance vector of C1' atoms of the second basepair (*lower double arrow*) and the cross product of this vector and the axis connecting the midpoints of the two vectors (*linear helical axis*). The projection is shown as dotted lines in the right panel. The twist angle between the two basepairs with respect to the linear helical axis is indicated as a torque arrow (*right panel*).

TABLE 1 Optimal twist and fourth-order polynomial fit of the calculated PMF for twist deformations

Sequence (5'–3')	Optimal twist (τ_o)	k_2 (kcal mol^{-1} deg^{-2})	k_3 (kcal mol^{-1} deg^{-3})	k_4 (kcal mol^{-1} deg^{-4})
CGCG**AATT**CGCG	32.7°	0.054	0.0040	0.0015
CGCG**TATA**CGCG	32.6°	0.030	0.0025	0.0010
CGCG**CGCG**CGCG	31.0°	0.071	−0.0006	−0.0010
CGCG**GATC**CGCG	30.8°	0.053	−0.0001	−0.0007
CGCG**CATG**CGCG	30.9°	0.049	−0.0020	−0.0010
CGCG**CTAG**CGCG	30.9°	0.053	0.0002	−0.0008

The calculated PMF for twist deformation τ (Fig. 3) was fitted to a fourth-order polynomial of the form $f(\tau) = k_2 (\tau - \tau_o)^2 + k_3 (\tau - \tau_o)^3 + k_4 (\tau - \tau_o)^4$.
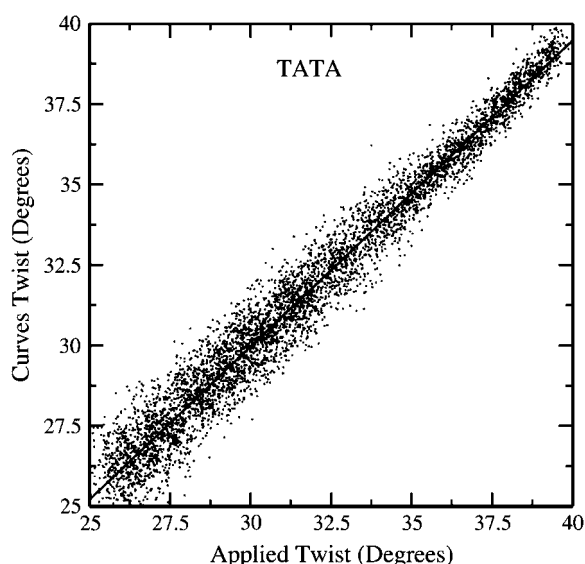
FIGURE 2   Correlation of twist (per basepair step) calculated using the program *Curves* (40,41) and the twist as defined in Fig. 1 (given as average per-bp step twist instead of per 9-bp step as indicated in Fig. 1) that has been used as twist-restraining coordinate during the MD simulations. The data (for the central TATA case) covers the whole range of twist-restraining simulations from 25–40° per basepair step.

RESULTS AND DISCUSSION

Potential of mean force for DNA twist deformation

Molecular dynamics umbrella sampling calculations including a twist-restraining potential were performed on six B-DNA oligonucleotides with different central basepairs (bp) and GC-rich flanking sequences (Table 1). The twist-restraining potential (Fig. 1, Materials and Methods) was applied between the second and eleventh basepairs (one before terminal bp). Within the five central steps of these oligonucleotides, all possible bp steps are included at least once. The GC-rich flanking sequences served to stabilize the duplex structure of all central sequences to the same extent. During simulations including the twist restraint, the reference twist, as defined in Fig. 1 along 9-bp steps, was changed in increments of 5° with 0.2-ns equilibration and 1-ns data-gathering per step using a quadratic restraining potential. To avoid any local structural perturbations of the helix a soft potential with a force constant of 0.06 kcal mol^{-1} deg^{-2} was used. The small restraining force constant allows also for sufficient overlap between twist-angle distribution curves at each reference twist for the calculation of a PMF along the twist-restraining coordinate using the WHAM method (42,43). It is important to note that the current twist-restraining angle is only an approximation to the "real" twist because it is calculated with respect to a linear helical axis along the DNA. To compare the current approximate twist coordinate with a more accurate definition that also accounts for a possible curved helical axis, it was compared to the twist obtained using the program *Curves* (40,41). For the range of twist

deformations considered in this study, the twist-restraining coordinate correlated very well with a more accurate twist of the DNA calculated using the *Curves* program (Fig. 2).

The range of twist values covered during the simulations was limited to an average 25–40° per bp step (Fig. 3). Further over-twisting of the DNA beyond these limits led in all cases to a steep rise of the calculated PMF due to sterical strain (see Fig. 3). Untwisting below ~25° per bp resulted in the onset of significant structural changes (stable transitions) of the DNA discussed in the last paragraph of Results and Discussion. These structural changes occurred spontaneously and asymmetrically starting at one end of the DNA and require much longer simulations to achieve convergence of the associated free-energy changes. The limitation to an average range of ~25–40° per bp step allowed a very good convergence of the free energy curves (compare *dotted*, *dashed*, and *bold lines* in Fig. 3 that correspond to different simulation times for each twist reference value). For all sequences and most parts of the plots, the final drift of the free energy curves was smaller than 0.5 kcal mol^{-1}. The basic shape of the free energy curves was similar for all sequences (Fig. 3) with a minimum in the free energy curves in the range of ~31–33°, which is ~3–5° smaller than the experimentally observed 36° per bp step. Such smaller average twist angles compared to standard B-DNA were also observed in unrestrained MD simulations using the same force field (31.5–33° per bp step, data not shown). It agrees also with previous MD-simulation studies on B-DNA using the AMBER force field, indicating that both the PARM94 (44) and, to a lesser degree, the current PARM99 force-field parameters (36,37), result in slightly under-twisted average structures during MD
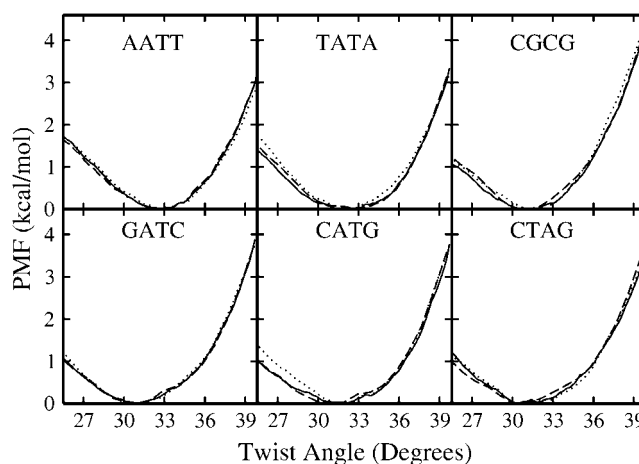

FIGURE 3   Potential of mean force (PMF) of twist deformations obtained during umbrella-sampling molecular dynamics simulations (*central sequences* are indicated in each panel). The calculated PMF (using the WHAM approach (42)) is plotted versus the applied twist-restraining angle for 0.4 ns (*dotted line*), 0.8 ns (*dashed line*), and 1 ns (*continuous line*) data gathering times (for each value of the twist-restraining coordinate), respectively. Note, that the twist is given per-bp step (divided by 9), and not per 9-bp steps as shown in Fig. 1.

simulations (32,33,36)—which also implies that these force fields do not reproduce the sequence-dependent equilibrium twist of B-DNA.

The optimal twist differs slightly between the six sequences (Table 1). As expected, the calculated free energy curves are not symmetric with respect to the twist minimum. Over-twisting of the DNA causes generally a stronger increase of the free energy compared to untwisting of the DNAs. The calculated PMFs can be approximated very well by a fourth-order polynomial (Table 1). The quadratic term which dominates for small twist deformations indicates a range of twist elastic constants between ~0.03 and ~0.07 kcal mol^{-1} deg^{-2}. The calculated range of twist elastic constants is in very good agreement with available experimental data (18–21) and results of unrestrained DNA simulations that obtain effective force constants for twist deformations from twist distribution functions (29–31). It translates to a range of twist fluctuations per bp step ($= sqrt$ ($R T/ c$), where R is the gas constant, T is the temperature, and c is the elastic constant) at room temperature of 3–5°. In terms of overall twist flexibility near the optimal twist, the central TATA sequence was the most flexible, followed by CATG, CTAG, and GATC (Table 1). The stiffest sequences, with respect to twist, are the DNAs with central AATT and central GCGC sequence. The overall modest variation of the effective twist flexibility among the various sequences agrees with the experimental observation based on DNA cyclization experiments (17–19) and time-resolved fluorescence polarization anisotropy (20,21).

Twist flexibility of individual basepair steps

Although the average twist flexibility/rigidity over a range of 10 basepairs (9-bp steps) showed only modest variation, the response of the individual bp steps on external twist stress is highly nonuniform (Figs. 4 and 5). To first illustrate the non-uniform response of basepair steps, the average twist (calculated using *Curves*) of the five central basepair steps (for the central sequences AATT, TATA, and CTAG) has been plotted for five ranges of external twist stress (Fig. 4). The height of each bar indicates the actual average twist for the corresponding basepair step at high or medium over-twisting (*first two rows* of *bars*), low twist stress (*middle row*), and medium or high untwisting stress (*last two rows* in Fig. 4). Interestingly, several bp steps indicate only very small average twist changes over a large range of external twist stress (e.g., AT or GC steps). However, other steps, for example, the TA or TG basepair steps, showed a very significant twist deformability (average twist can vary between ~22° and ~42°) in all investigated sequences (compare central TATA and CTAG cases). This was also observed for other pyrimidine/purine steps whereas much smaller twist deformabilities were found for all purine/pyrimidine steps and to a lesser degree for purine/purine (pyrimidine/pyrimidine) steps (Fig. 4). The range of twist deformations observed for each basepair step (Fig. 5) allows us to qualitatively order the
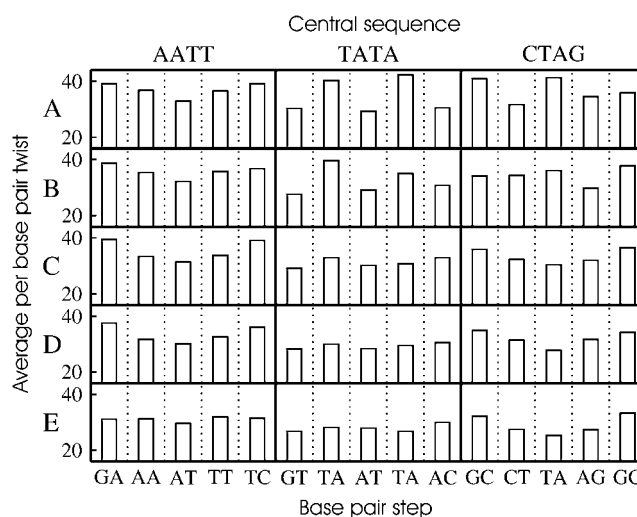

FIGURE 4 Average twist per basepair step versus applied twist stress. Each bar indicates the average twist per basepair (for the basepairs indicated on the *x* axis) along the central five basepair steps of three example DNA oligo-nucleotides (*central sequence* given on *top* of each panel). The five rows correspond to five levels of twist stress. (*A*) The first row corresponds to strong over-twisting along the nine central bp steps that translates to an average applied per-basepair twist of 37–40°. The other four rows correspond to applied per-basepair twists of 34–37° (*B*, slight over-twisting), 31–34° (*C*, close to equilibrium), 28–31° (*D*, slight untwisting), and 25–28° (*E*, strong untwisting), respectively.

basepair-step twist deformability (Table 2). The largest flexibility was found for the TA and CA/TG step followed by the CG steps. The GG/CC step followed by the GA/TC step showed the largest deformability for the purine/purine steps (smallest: AA/TT). Very similar small deformability was found for all purine/pyrimidine steps (only 3–4° variation upon an average external twist change of 15°, Fig. 5). The order of bp step twist flexibility agrees qualitatively very well with available data on the twist distribution in experimental B-DNA crystal structures (7–15) and also with results of unrestrained MD simulations (29–33). It also indicates that a DNA reacts on an external twist stress by a highly nonuniform relaxation at the basepair step level. Most of the external twist stress is absorbed by the efficient twist relaxation of pyrimidine/purine basepair steps and to a considerably lesser degree by other steps. Longer stretches of natural DNA contain usually many different basepair steps including pyrimidine/purine steps such that the overall response of DNA segments to external torques is relatively uniform (21). However, one should also keep in mind that the total twist deformability of a DNA molecule may not just be the sum of individual basepair twist deformabilities. For example, it has been shown for RNA (45,46) that twist deformations at a given basepair step are anticorrelated to twist deformations at neighboring steps (local over-twisting at one step promotes under-twisting at adjacent steps). An effective twist force constant for a stretch of DNA is determined by the flexibility of individual steps and the degree of covariation with respect

TABLE 2 Twist flexibility of basepair steps and coupling to slide and roll

Basepair step	Local twist range (°)	Slide-twist coupling (Å per degrees)	Roll-twist coupling (degrees per degrees)
AA/TT	30–37	0.014	−0.83
GG/CC	28–37	0.044	−0.77
GA/TC	31–41	0.028	−0.71
AG/CT	28–34	0.035	−0.83
TA	24–42	0.036	−1.13
CG	26–40	0.030	−0.89
CA/TG	24–42	0.025	−0.78
GC	34–37	0.024	−1.03
AT	29–32	−0.030	−1.30
GT/AC	29–32	0.004	−1.05

The slide-twist coupling and roll-slide coupling corresponds to the slope of the linear fits shown in Fig. 6. Note that the coupling coefficients of the last three rows have a large uncertainty due to the small range of covered twist angles.

to neighboring steps (other helical parameters may also come into play if the DNA is not straight).

Twist coupling to other helical parameters and nucleic acid backbone structure

Besides twist, the helical parameters' slide and roll are the most variable in DNA (4,9–15). Also, the observed coupling between twist and slide or roll in known DNA structures is much stronger compared to the coupling to the helical parameters tilt and shift (4,9–12) and only the former are considered here. The extraction of correlations between helical parameters using available DNA oligonucleotide structures or unrestrained MD simulations requires large data sets to obtain statistically meaningful results. An advantage of the present simulation approach is that any average helical parameter and its dependence on twist can be directly extracted and plotted from simulations using different twist-restraining coordinates. The analysis of DNA crystal structures indicates a negative correlation between roll and twist (4) Such negative correlation was also found in the present study for every basepair step (Fig. 6 *a*). Interestingly, the degree of correlation (ratio of roll/twist changes) showed only a modest variation (Table 2). However, pyrimidine/purine steps showed overall much larger variation in twist and coupled to this also a much greater variation in roll (−10 to +20°). The correlation and range of twist/roll deformations is in very good agreement with experimental data (4). Overall, a positive correlation between twist and the helical variable slide was found for most basepair steps, again in good agreement with experiment (4,9–12). However, for some steps (AG, AT, GT, and AC) no accurate correlation can be extracted. This was largely due to the small changes in twist at the corresponding basepair steps during the simulations (Fig. 6 *b*).

As expected from the observed coupling of twist changes to other helical parameters—in particular, roll—the induced twist deformation also lead to an overall slight average
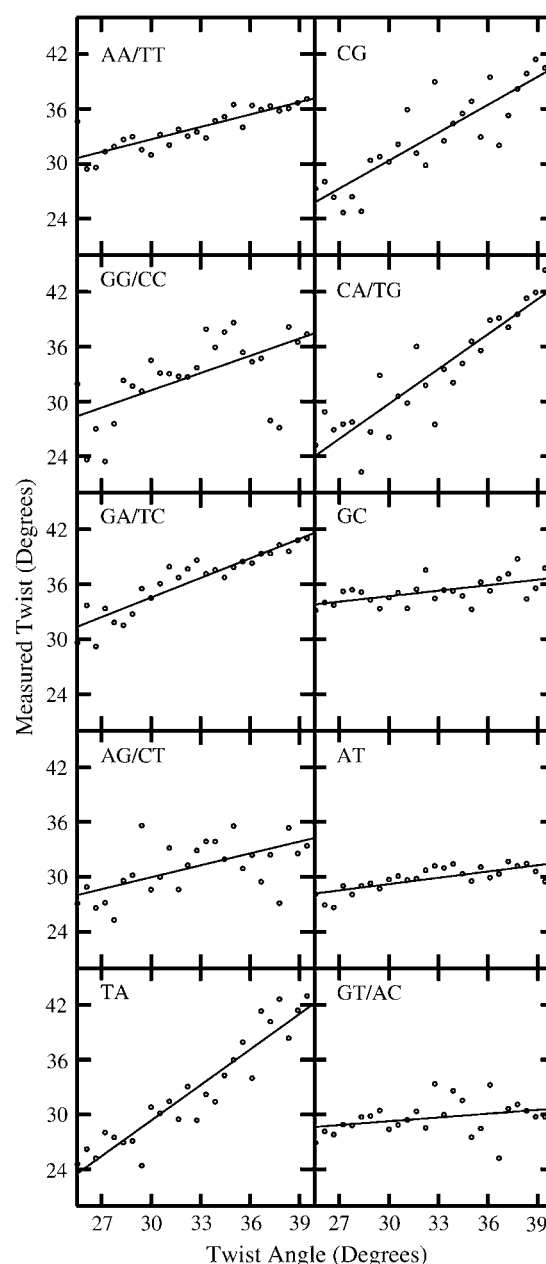

FIGURE 5 Local twist of each of the 10 possible basepair steps versus applied twist (per basepair step along each DNA). Each panel represents the average twist (per indicated basepair step) from all simulations (at the indicated applied twist) on the six different DNA oligonucleotides (Table 1).

bending of the DNAs (Fig. 7 *a*) ranging from ∼10° (with an average restraining twist of 40°) to ∼40° in case of a restraining twist of ∼25° (Fig. 7 *a*). Note that even in unrestrained simulations, a B-DNA molecule for entropic reasons is, on average, bent (even if the straight form is the energetically most favorable form). DNA untwisting also resulted in an increase of the minor groove size (Fig. 7 *b*). As an example, the observed structural changes are illustrated for the TATA case in Fig. 8. The over-twisted structure has a narrow minor
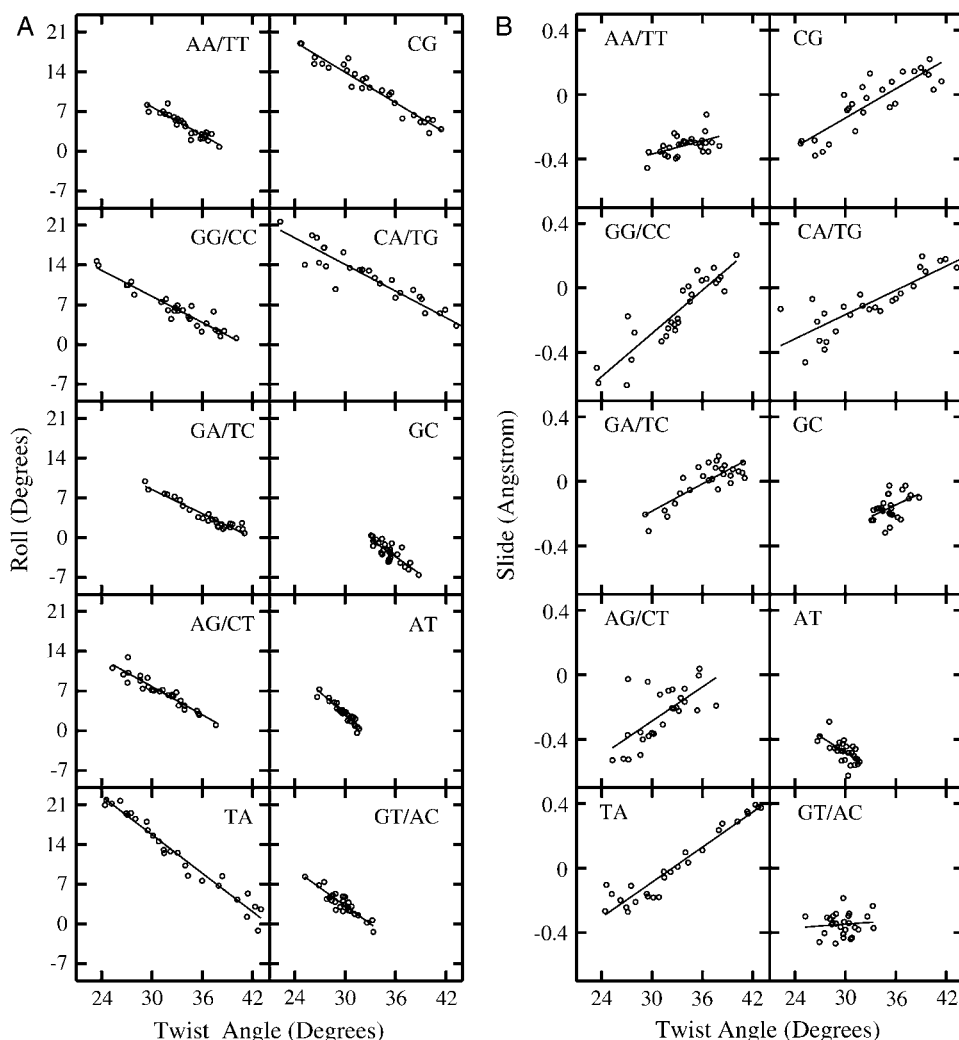
FIGURE 6 Correlation of helical parameters roll (*A*) and slide (*B*) with the twist angle obtained using *Curves* (40,41) at each of the 10 possible basepair steps (data obtained from twist restraining simulations on all six oligonucleotides, see Table 1).

groove with a relatively straight helical axis. The untwisted structure has a wider minor groove and a narrower major groove compared to standard B-DNA more typical for A-form structures (Fig. 8). As expected, overall the untwisting increases the A-form character of the DNAs. Another indicator of the increased A-form character upon untwisting of the DNA is the observed shift of the distribution of the deoxyribose δ-dihedral angles (of the central parts of the DNA) from values characteristic for B-DNA (at high over-twisting stress) to smaller values with contributions characteristic for A-form (δ-dihedral angle at ~85°) upon untwisting (Fig. 9). Interestingly, the γ-dihedral angle distribution stayed close to the distribution characteristic for B-DNA (+*gauche*, Fig. 9). It has been reported that during very long MD simulations of B-DNA using the AMBER force-field transitions to backbone structure with α/γ, flips (crank shift transitions) may occur (47). This was not observed in the present simulations, possibly because the (independent) simulations per each twist-restraining window were, overall, relatively short (<2 ns). However, as indicated in Fig. 9 (*lower two panels*), a

number of B$_{II}$ states (a correlated shift of nucleic acid backbone ε- and ζ-dihedral angles from t to $-g$ and $-g$ to t, respectively) were observed (~10% B$_{II}$). This is slightly larger than what has been found in unrestrained simulations (~6% B$_{II}$, (33)) and likely due to the fact that B$_I$-B$_{II}$ transitions can affect the twist of DNA. However, no clear correlation between B$_{II}$-state frequency and twist stress in the present twist range was observed (Fig. 9).

Conformational changes upon extensive untwisting

The purpose of this study was the analysis of free energy changes and DNA structural changes upon application of twist stress not too far from the equilibrium twist. The restriction was necessary because the present twist-coordinate is only appropriate in case of modest global conformational changes of the DNA. In addition, it was observed that the calculated free energy changes did not converge in the case of severe untwisting of DNA. Since, in this study, each DNA
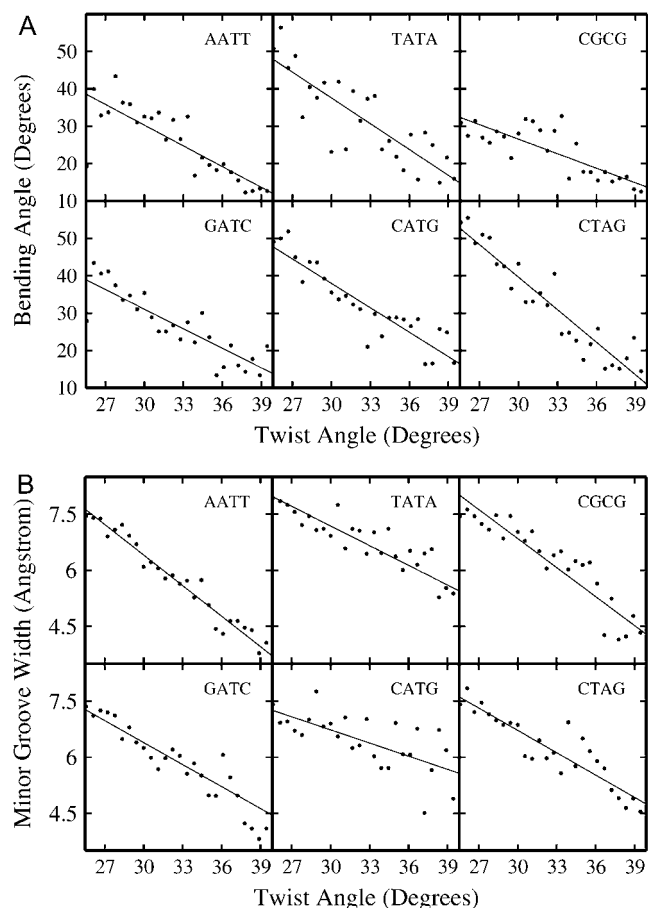
FIGURE 7 Correlation of bending (*A*) and minor groove width (*B*) versus applied restraining twist (per basepair step along each DNA). Global bend angle and minor groove width were calculated using *Curves* (40,41).
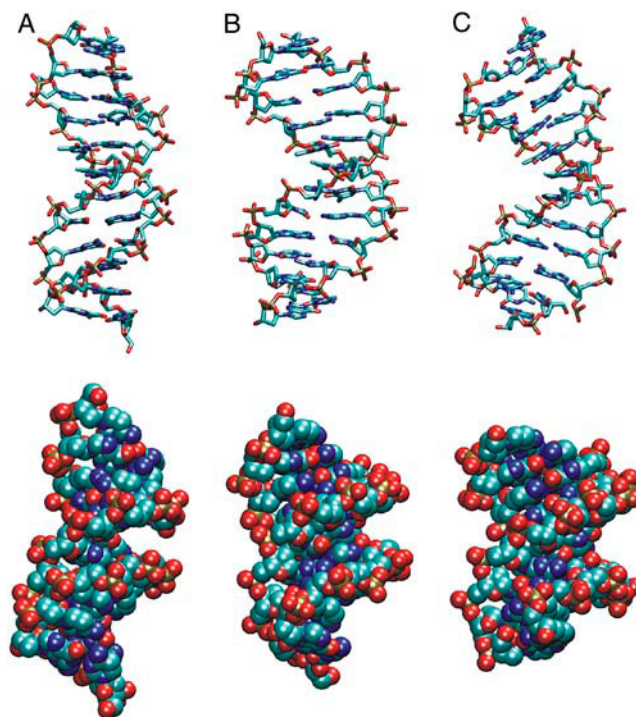

FIGURE 8 Comparison of average DNA structures (central TATA case) during restrained MD simulations at a twist restraint corresponding to 40° (*A*), 33° (*B*), and 25° (*C*) per bp step, respectively. The view in the case of the upper set of panels (*stick model*, atomic color code) is perpendicular to the helical axis (*major groove* to the *left*). For the lower set of panels (van der Waals representation), the view is along the central portion of the DNA minor-groove.

molecule consisted of self-complementary strands, it is expected that for fully reversible conformational deformations, the same behavior of identical basepair steps at symmetric positions in the structure should be observed. However, upon untwisting below an average applied twist of 25°, spontaneous untwisting transitions, starting from one end of the helix, were observed (Fig. 10). Such spontaneous untwisting transition beginning at one side of the DNA reduces the overall twist tension and therefore stabilizes a higher, close to B-DNA equilibrium, twist at the other parts of the helix (Fig. 10 *b*). Once such transition has occurred, the uniform distribution of twist tension along the DNA is lost, and at least on the present simulation timescale, no spontaneous redistribution of the twist tension occurs (no driving force). For the case shown in Fig. 10, the twist-restraining reference value (per bp step) was 20°. The DNA splits into a part with a twist only slightly below the equilibrium twist (of B-DNA) and one part with significantly reduced twist per bp step (~12°; Fig. 10 *b*). The backbone adopts a zigzag-type structure accompanied by changes in the backbone dihedral angles including α/γ flips and B_I-B_{II} transitions. The base-

pairs remain, however, in a stacked geometry but the helical structure changes dramatically adopting a geometry with largely open and well-accessible minor and major grooves (Fig. 10 *a*). It should be noted that the possibility that such a transition is a result of force-field artifacts cannot be excluded. Since the conformational transition involves significant changes of the helical structure of the DNA, a convergence of calculated free energies cannot be achieved on the present timescale. This would require us to cover reversible back-and-forth twist transitions along the whole DNA structure. Nevertheless, the current simulations allowed us to estimate the untwisting stress on a DNA molecule required for the onset of such transitions. Transitions were observed already at a reference twist per basepair step below 20–25° that is ~7–12° (or ~25%) smaller than the equilibrium twist angle of B-DNA (assuming ~32–33° as equilibrium twist for the current force field). An untwisting stress of ~10° per bp step translates to an unwinding of DNA by one turn every 36-bp steps. This is considerably larger than the typical superhelical stress of circularly closed DNA in vivo (~1 turn every 200 steps). In addition, on a larger length scale, much of the twist stress is absorbed into superhelical turns in DNA. However, within complexes of DNA with proteins, it might well be possible that locally a
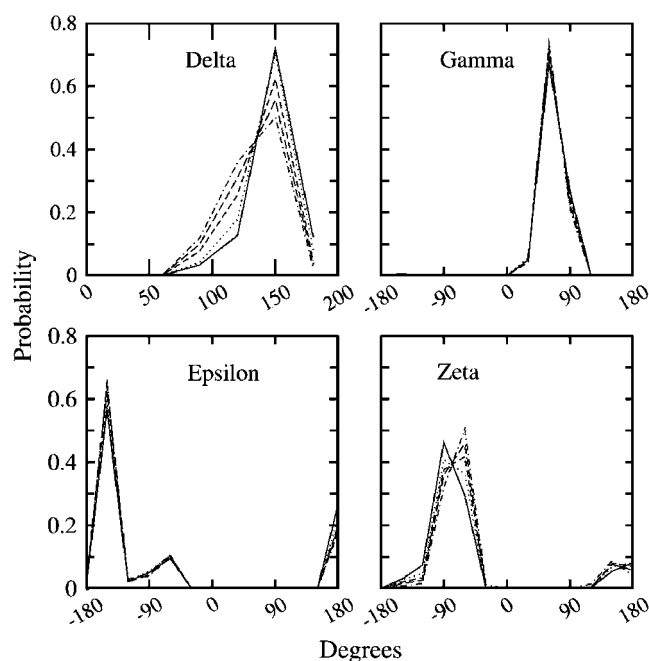
FIGURE 9   Nucleic acid backbone dihedral angle distributions (TATA case) for the central-six basepair steps during the data-gathering simulation period. Continuous line indicates distribution at high twist stress, 37–40° (per basepair step); the dotted line, 34–37°; short-dashed, 31–34°; long-dashed, 28–31°; and dotted-dashed, 25–28°, respectively.

large twist stress of $\sim$10° per bp step can be achieved, possibly leading to structural transitions similar to those seen in this study. The analysis of these structural transitions and the dependence of such transitions on the force-field parameters will be subject of a future study.

CONCLUSIONS

Understanding DNA deformability in particular of the DNA-helical twist is of fundamental importance to understand processes like DNA recognition, packing, transcription, and replication. In this study, a molecular dynamics umbrella sampling approach was used to study systematically, on several different DNA molecules, the free energy change associated with an over- or untwisting of a segment of DNA. It was possible to extract the shape of the free energy curves versus applied twist restraint, and qualitatively similar curves for the six tested DNA molecules were observed. The approach goes beyond previous unrestrained simulations that do not allow us to directly extract the free energy change associated with DNA deformations. It also complements experimental single molecule studies (22) mostly performed on long DNAs that largely relax applied torsional stress through supercoiling and approaches that evaluate DNA flexibility indirectly from analyzing experimental DNA crystal structure (4–12). The current results are in very good agreement with available experimental data on the overall twist flexibility of DNA as well as on the local per-bp step
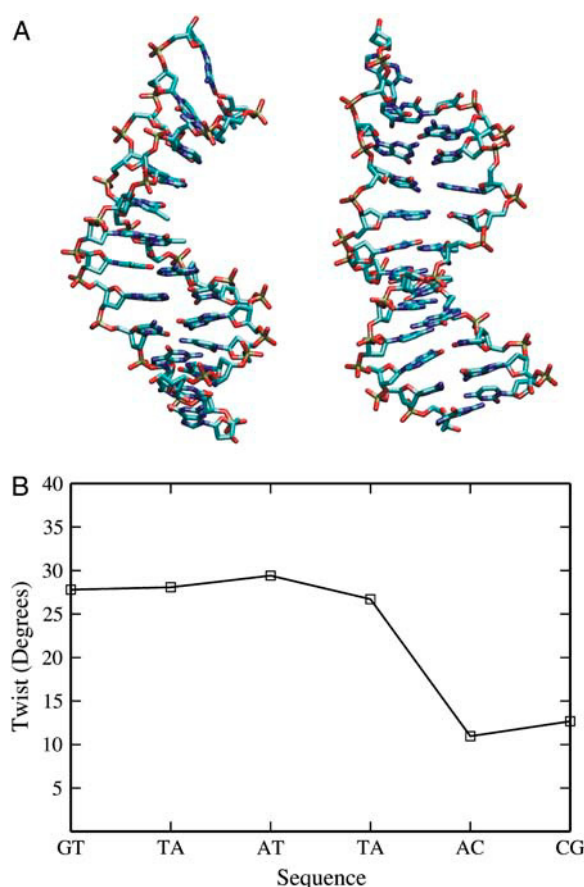

FIGURE 10   (*A*) Average structure of a DNA oligonucleotide (central TATA sequence) during a twist-restraining simulation (1 ns data gathering time) with a twist-restraint reference of 20° per bp step. The two views in panel *A* differ by a 90° rotation around the helical axis. (*B*) Average twist per bp step (calculated using *Curves*) along basepairs 3–8 of the DNA oligonucleotide. The structures are available from the corresponding author upon request.

flexibility and the coupling to other helical parameters. This result indicates that the structural variation seen in DNA crystal structures does indeed reflect to a significant degree the DNA flexibility in solution. The simulation study indicates that the strongly nonuniform local response to external twist stress can significantly alter the local arrangement of chemical groups recognized by ligands. In addition, twist stress can alter the overall shape of a DNA segment (Fig. 8), including DNA bending and groove deformation again strongly modulating the accessibility by proteins and other ligands. Interestingly, the onset of a structural transition of the double helix to a structure with a strongly reduced twist compared to B-DNA and opened minor and major grooves was observed during extensive DNA untwisting simulations. The significance of this transition will be subject of a future study.

REFERENCES

1. Hagerman, P. J. 1990. Flexibility of DNA. *Annu. Rev. Biochem.* 59: 755–781.

2. von Hippel, P. H., W. A. Rees, K. Rippe, and K. S. Wilson. 1996. Specificity mechanisms in the control of transcription. *Biophys. Chem.* 59:231–246.

3. Rhodes, D., J. W. Schwabe, L. Chapman, and L. Fairall. 1996. Before an understanding of protein-DNA recognition. *Philos. Trans. R. Soc. Lond. B Biol. Sci.* 351:501–509.

4. Olson, W. K., A. A. Gorin, X.-J. Lu, L. M. Hock, and V. B. Zhurkin. 1998. DNA sequence-dependent deformability deduced from protein-DNA crystal complexes. *Proc. Natl. Acad. Sci. USA.* 95:11163–11168.

5. Willenbrock, H., and D. W. Ussery. 2004. Chromatin architecture and gene expression in *Escherichia coli. Genome Biol.* 5:252.

6. Travers, A. A., and G. Muskhelishvili. 2005. Bacterial chromatin. *Curr. Opin. Genet. Dev.* 15:507–514.

7. Calladine, C. R. 1980. The principles of sequence-dependent flexure of DNA. *J. Mol. Biol.* 192:907–918.

8. Hunter, C. A. 1993. Sequence-dependent DNA structure. The role of base stacking interactions. *J. Mol. Biol.* 230:1025–1054.

9. Gorin, A. A., V. B. Zhurkin, and W. K. Olson. 1995. B-DNA twisting correlates with basepair morphology. *J. Mol. Biol.* 247:34–48.

10. El Hassan, M. A., and C. R. Calladine. 1995. The assessment of the geometry of dinucleotide steps in double-helical DNA: a new local calculation scheme. *J. Mol. Biol.* 251:648–664.

11. El Hassan, M. A., and C. R. Calladine. 1997. Conformational characteristics of DNA: empirical classifications and a hypothesis for the conformational behaviors of dinucleotide steps. *Philos. Trans. R. Soc. Lond. A.* 355:43–100.

12. Packer, M. J., M. P. Dauncey, and C. A. Hunter. 2000. Sequence-dependent DNA structure: tetranucleotide conformational maps. *J. Mol. Biol.* 295:85–103.

13. Travers, A. A., and J. M. T. Thompson. 2004. An introduction to the mechanics of DNA. *Philos. Trans. R. Soc. Lond. A.* 362:1265–1279.

14. Olson, W. K., D. Swigon, and B. D. Coleman. 2004. Implications of the dependence of the elastic properties of DNA on nucleotide sequence. *Philos. Trans. R. Soc. Lond. A.* 362:1403–1422.

15. Travers, A. A. 2004. The structural basis of DNA flexibility. *Philos. Trans. R. Soc. Lond. A.* 362:1423–1438.

16. Deremble, C., and R. Lavery. 2005. Macromolecular recognition. *Curr. Opin. Struct. Biol.* 15:171–175.

17. Hagerman, P. J. 1985. Analysis of ring-closure probabilities of isotropic worm-like chains: application to DNA. *Biopolymers.* 24:1881–1897.

18. Crothers, D. M., J. Drak, J. D. Kahn, and S. D. Levene. 1992. DNA bending, flexibility, and helical repeat by cyclization kinetics. *Methods Enzymol.* 212:3–29.

19. Kahn, J. D., E. Yun, and D. M. Crothers. 1994. Detection of localized DNA flexibility. *Nature.* 368:163–166.

20. Shibata, J. H., B. S. Fujimoto, and J. M. Schurr. 1985. Rotational dynamics of DNA from 10^{-10} to 10^{-5} seconds: comparison of theory with optical experiments. *Biopolymers.* 24:1909–1930.

21. Fujimoto, B. S., and J. M. Schurr. 1990. Dependence of the torsional rigidity of DNA on base composition. *Nature.* 344:175–178.

22. Bustamante, C., Z. Bryant, and S. B. Smith. 2003. Ten years of tension: single-molecule DNA mechanics. *Nature.* 421:423–426.

23. Cheatham III, T. E., and M. A. Young. 2001. Molecular dynamics simulation of nucleic acids: successes, limitations, and promise. *Biopolymers.* 56:232–256.

24. Giudice, E., and R. Lavery. 2002. Simulations of nucleic acids and their complexes. *Acc. Chem. Res.* 35:350–357.

25. MacKerell, A. D. 2004. Empirical force fields for biological macromolecules: overview and issues. *J. Comput. Chem.* 25:1584–1604.

26. Cheatham, T. E. 2004. Simulation and modeling of nucleic acid structure, dynamics and interactions. *Curr. Opin. Struct. Biol.* 14: 360–367.

27. Flatters, D., and R. Lavery. 1998. Sequence-dependent dynamics of TATA-box binding sites. *Biophys. J.* 75:372–381.

28. Foloppe, N., and A. D. MacKerell. 2000. All-atom empirical force field for nucleic acids. 1. Parameter optimization based on small molecule and condensed phase macromolecular target data. *J. Comput. Chem.* 21:86–104.

29. Lankas, F. 2003. DNA sequence-dependent deformability-insights from computer simulations. *Biopolymers.* 73:327–339.

30. Lankas, F., J. Sponer, J. Langowski, and T. E. Cheatham. 2003. DNA deformability at the basepair level. *J. Am. Chem. Soc.* 126:4124–4125.

31. Lankas, F., J. Sponer, J. Langowski, and T. E. Cheatham. 2004. DNA basepair step deformability inferred from molecular dynamics simulations. *Biophys. J.* 85:2872–2883.

32. Beveridge, D. L., G. Barreiro, K. S. Byun, D. A. Case, T. E. Cheatham 3rd, S. B. Dixit, E. Giudice, F. Lankas, R. Lavery, J. H. Maddocks, R. Osman, E. Seibert, H. Sklenar, G. Stoll, K. M. Thayer, P. Varnai, and M. A. Young. 2004. Molecular dynamics simulations of the 136 unique tetranucleotide sequences of DNA oligonucleotides. I. Research design and results on *d*(CpG) steps. *Biophys. J.* 87:3799–3813.

33. Dixit, S. B., D. L. Beveridge, D. A. Case, T. E. Cheatham III, E. Giudice, F. Lankas, R. Lavery, J. H. Maddocks, R. Osman, H. Sklenar, K. M. Thayer, and P. Varnai. 2005. Molecular dynamics simulations of the 136 unique tetranucleotide sequences of DNA oligonucleotides. II. Sequence context effects on the dynamical structures of the 10 unique dinucleotide steps. *Biophys. J.* 89:3721–3740.

34. Case, D. A., D. A. Pearlman, J. W. Caldwell, T. E. Cheatham III, W. S. Ross, C. L. Simmerling, T. A. Darden, K. M. Merz, R. V. Stanton, A. L. Cheng, J. J. Vincent, M. Crowley, V. Tsui, R. J. Radmer, Y. Duan, J. Pitera, I. Massova, G. L. Seibel, U. C. Singh, P. K. Weiner, and P. A. Kollman. 2003. AMBER 8. University of California, San Francisco, CA.

35. Jorgensen, W., J. Chandrasekhar, J. Madura, R. Impey, and M. Klein. 1983. Comparison of simple potential functions for simulating liquid water. *J. Chem. Phys.* 79:926–935.

36. Cheatham III, T. E., P. Cieplak, and P. A. Kollman. 1999. A modified version of the Cornell et al. force field with improved sugar pucker phases and helical repeat. *J. Biomol. Struct. Dyn.* 16:845–862.

37. Duan, Y., C. Wu, S. Chowdhury, M. C. Lee, G. Xiong, W. Zhang, R. Yang, P. Cieplak, R. Luo, T. Lee, J. Caldwell, J. Wang, and P. Kollman. 2003. A point-charge force field for molecular mechanics simulations of proteins based on condensed-phase quantum mechanical calculations. *J. Comput. Chem.* 24:1999–2012.

38. Darden, T. A., D. M. York, and L. Pedersen. 1993. Particle mesh Ewald: an *N*log*N* method for Ewald sums in large systems. *J. Chem. Phys.* 98:10089–10092.

39. Miyamoto, S., and P. A. Kollman. 1992. SETTLE: an analytical version of the SHAKE and RATTLE algorithm for rigid water models. *J. Comput. Chem.* 13:952–962.

40. Lavery, R., and H. Sklenar. 1988. The definition of generalized helicoidal parameters and of axis curvature for irregular nucleic acids. *J. Biomol. Struct. Dyn.* 6:63–91.

41. Lavery, R., and H. Sklenar. 1988. Defining the structure of irregular nucleic acids: conventions and principles. *J. Biomol. Struct. Dyn.* 6: 655–667.

42. Kumar, S., D. Bouzida, R. H. Swendsen, P. A. Kollman, and J. M. Rosenberg. 1992. The weighted histogram analysis method for free-energy calculations on biomolecules. I. The method. *J. Comput. Chem.* 13:1011–1021.

43. Grossfield, A. 2003. http://dasher.wustl.edu/alan.

44. Cornell, W. D., P. Cieplak, C. I. Bayley, I. R. Gould, K. M. Merz, D. M. Ferguson, D. C. Spellmeyer, T. Fox, J. W. Caldwell, and P. A. Kollman. 1995. A second generation force field for simulation of proteins, nucleic acids and organic molecules. *J. Am. Chem. Soc.* 117:5179–5197.

45. Zacharias, M., and H. Sklenar. 2000. Conformational deformability of RNA: a harmonic mode analysis. *Biophys. J.* 78:2528–2542.

46. Zacharias, M. 2000. Comparison of molecular dynamics and harmonic mode calculations on RNA. *Biopolymers.* 54:547–560.

47. Barone, F., F. Lankas, N. Spackova, J. Sponer, P. Karran, M. Bignami, and F. Mazzei. 2005. Structural and dynamic effects of single 7-hydro-8-oxoguanine bases located in a frameshift target DNA sequence. *Biophys. Chem.* 118:31–41.